PAPER

Check for updates

Development and evaluation of *N*-acetyl cysteine-grafted polyamidoamine dendrimers for enhanced brain delivery of donepezil hydrochloride

Teeja Suthar [ID] and Keerti Jain [ID] *

Donepezil hydrochloride (DPZ) is a USFDA-approved, selective and non-competitive, centrally acting acetylcholinesterase inhibitor used for the clinical management of dementia associated with mild-to-moderate Alzheimer's disease (AD). However, treatment with DPZ is usually associated with various peripheral adverse effects, which necessitate the use of ligand-mediated targeted delivery approaches for selective delivery to the target site. This study reports the synthesis and evaluation of *N*-acetyl cysteine (NAC)-conjugated poly(amidoamine) G4 (PAMAM G4) dendrimers for brain-targeted delivery of DPZ. Fourier-transform infrared (FTIR) and nuclear magnetic resonance (NMR) spectroscopy were used to confirm the conjugation of NAC to PAMAM G4 dendrimers. DPZ was loaded onto PAMAM G4 and the NAC-G4 conjugate, and % drug entrapment, loading efficiency, and release behavior were determined. The cell viability assay showed enhanced viability with DPZ on incorporation into the NAC-G4 conjugate. Furthermore, we observed a higher peak plasma concentration and mean residence time of DPZ from the dendrimeric conjugate in pharmacokinetic studies. The DPZ-loaded ligand-conjugated dendrimeric conjugate holds promise as a potential strategy for the treatment of AD.

1. Introduction

Brain disorders like Alzheimer's disease (AD), Parkinson's disease, and malignancies are on the rise and are most challenging to treat. According to global estimates, a new case of dementia is reported approximately every 3 seconds worldwide. Over 55 million people worldwide were living with dementia in the year 2020, and it is projected to reach 78 million in 2030 and 139 million in 2050.[1] Alzheimer's disease (AD) is the most common type of dementia and accounts for 60–80% of the cases. AD is a complex, progressive neurodegenerative disorder that slowly destroys memory, cognition, and thinking skills.[2,3] It is generally characterized by intracellular abnormal deposition of amyloid beta (Aβ) plaques and extracellular accumulation of neurofibrillary tangles (NFTs) of hyperphosphorylated Tau protein.[4,5] The Center for Disease Control and Prevention (CDC) mentioned in one of its reports that the excess mortality in older adults due to all causes was very high in 2020 compared with those in previous

years, and there were at least 42 000 more deaths from AD and other types of dementias in 2020 compared with those in the last five years. It is equally alarming that the death toll due to AD has increased over the years in comparison with various heart diseases, stroke, and cancer.[6]

Currently, there is no therapeutic treatment available that can reverse the progression of such a complex disease. Therapeutic strategies aimed at the pathophysiological aspect of this disease have given promising results in preclinical models but failed to produce the same in clinical practice.[7] One of the widely accepted hypotheses of AD, *i.e.*, cholinesterase hypothesis, suggests that the cognitive decline in AD is associated with cholinergic deficit, including loss of cholinergic neurons and a decrease in the level of the neurotransmitter acetylcholine (ACh). Acetylcholinesterase (AChE) inhibitors are generally prescribed for the clinical management of AD symptoms. They inhibit AChE or butyrylcholinesterase enzymes in the synaptic cleft and increase the levels of ACh at the synapse and provide symptomatic relief to AD patients.[8,9] Donepezil, rivastigmine and galantamine are some of the approved AChE inhibitors for the clinical treatment of AD.[10,11]

Donepezil (DPZ), a USFDA approved selective and non-competitive inhibitor of AChE, is widely prescribed for the treatment of dementia related to mild-to-moderate Alzheimer's

Drug Delivery and Nanomedicine Research Laboratory, Department of Pharmaceutics, National Institute of Pharmaceutical Education and Research (NIPER)-Raebareli, Lucknow, India. E-mail: keertijain02@gmail.com, keertijain.02@niperraebareli.edu.in

disease. Structurally, it consists of dimethoxy indanone linked *via* a methylene linker to the *N*-benzylpiperidine moiety. It is marketed under the trade name Aricept®. It is the mainstay drug used in the treatment of AD; however, it suffers from various clinically relevant peripheral cholinergic adverse effects, which necessitate its formulation into targeted drug delivery systems.[12–15]

Dendrimers are branched spheroid polymers widely used in drug delivery applications as novel carriers to deliver high payloads of drugs. Poly(amidoamine) G4 (PAMAM G4) dendrimers are amine terminated cationic dendrimers that have high drug loading abilities along with very low toxicity. Furthermore, they have tunable surfaces which allow easy functionalization with anionic ligands for targeted delivery applications. PAMAM dendrimers are widely investigated for brain-targeted drug delivery owing to their nanoscale size, high drug-loading capacity, and ease of surface functionalization. Their ability to traverse the blood–brain barrier through receptor- or adsorptive-mediated transport mechanisms makes them promising nanocarriers for central nervous system (CNS) therapeutics.[16–19]

Numerous nanocarrier systems have been explored to improve the brain delivery and therapeutic efficacy of DPZ, a widely used AChE inhibitor. Liposomes, solid lipid nanoparticles (SLNs), polymeric micelles, and dendrimer-based systems have shown promise in enhancing bioavailability and brain uptake of DPZ. For example, Singh *et al.* developed PAMAM dendrimer–DPZ conjugates with improved pharmacokinetics and biodistribution profiles, emphasizing the potential of dendritic carriers in AD therapy.[20] ApoE functionalized SLNs enhanced DPZ transport across *in vitro* BBB models, demonstrating receptor-mediated transcytosis.[21] More recently, PEG-based polymeric micelles were proposed as stealth carriers for DPZ, achieving desirable nanoscale properties and drug encapsulation efficiency.[22] These studies collectively underscore the potential of nanoparticulate systems for targeted CNS drug delivery and support the ongoing need for developing ligand-directed nanocarriers to further refine site-specific brain targeting.

N-Acetylcysteine (NAC), a cysteine derivative, serves as a precursor to the critical antioxidant glutathione in the brain. Its transport across the blood–brain barrier (BBB) is facilitated by specific SLC1 amino acid transporters, notably Alanine–Serine–Cysteine Transporter 2 (ASCT2), also known as SLC1A5. ASCT2 is a neutral amino acid transporter that mediates the sodium-dependent exchange of small neutral amino acids, including alanine, serine, cysteine, and glutamine. NAC, being an acetylated form of cysteine, retains structural similarities that allow it to be recognized by ASCT2. This structural compatibility facilitates its transport across cell membranes, including the BBB.[23,24] Functionalizing nanocarriers with NAC may facilitate their uptake into the brain through these transporter pathways and offer a promising strategy to enhance drug delivery across the BBB. Furthermore, the multivalent nature of dendrimers allows for multiple NAC molecules to be attached, increasing the potential for transporter-mediated uptake. These strategies leverage NAC's biochemical properties

to improve the delivery of drugs to the CNS, offering potential advancements in treating neurological disorders.

In this research work, we have explored the ability of NAC as a brain targeting ligand conjugated to PAMAM G4 dendrimers to effectively deliver DPZ to the brain. We propose that this NAC-conjugated PAMAM dendrimer will be able to deliver high payloads of DPZ in the brain and exert better therapeutic activity to manage the progression of AD.

2. Methodology

2.1. Materials

Donepezil hydrochloride, poly(amidoamine) G4, *N*-acetyl cysteine, *N*-ethyl-*N*′-(3-dimethylaminopropyl) carbodiimide hydrochloride (EDC), *N*-hydroxy succinimide (NHS), AChE from *Electrophorus electricus*, acetylthiocholine iodide (ATCI), and 5,5′-dithiobis(2-nitrobenzoic acid) (DTNB) were purchased from Sigma Aldrich, Bangalore, India. Chromatography grade acetonitrile, acetic acid, and triethylamine were purchased from Merck India Pvt. Ltd, Mumbai, India. SnakeSkin™ dialysis tubing 7k MWCO was purchased from ThermoFisher Scientific (Rockford, IL, USA). Triple-distilled water was obtained from the Milli-Q assembly of NIPER-R. All other chemicals and reagents were of analytical grade and used without further purification.

2.2. Synthesis of the NAC-G4 conjugate

Conjugation of the carboxyl group of NAC to the primary amine group of PAMAM G4 dendrimers was performed using EDC-NHS conjugation chemistry.[25] The conjugation scheme is depicted in Fig. 1. Briefly, 1 mole of PAMAM G4 dendrimer was dispersed in water and 50 moles of NAC were dissolved in 1 mL of water. The carboxylic acid group of NAC was activated by the addition of 60 moles each of EDC and NHS. After stirring the mixture for 30 minutes at room temperature, the PAMAM G4 solution was added dropwise, and the volume of the reaction mixture was made up to 5 mL. The reaction mixture was stirred overnight at room temperature and unreacted NAC, EDC and NHS were removed by dialyzing against excess amounts of water using a 7 kDa MWCO membrane. The resultant product was lyophilized and characterized using various spectroscopic techniques.

2.3. Characterization of the NAC-G4 conjugate

The lyophilized product was characterized for the confirmation of conjugation using FTIR and ^{1}H NMR spectroscopy. The FTIR spectra of PAMAM G4, NAC and NAC-G4 were recorded in the wavenumber range of 4000–600 cm^{-1}. Furthermore, the samples for ^{1}H NMR spectroscopy were prepared by dissolving PAMAM G4, NAC and NAC-G4 in deuterated dimethyl sulfoxide and the spectra were recorded using a 500 MHz JEOL Resonance ECZ500R (JEOL Ltd, Tokyo, Japan).
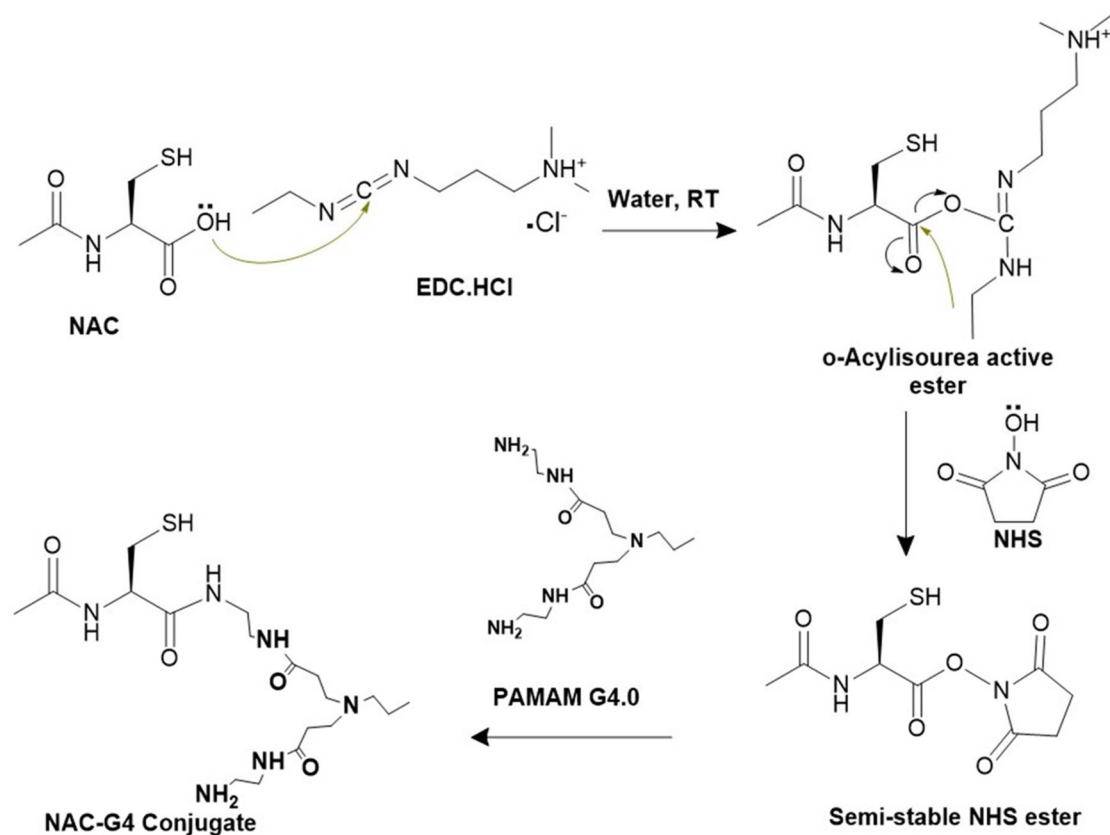
Fig. 1 Schematic representation of the conjugation scheme.

2.4. Dynamic light scattering studies

The average hydrodynamic diameter and apparent zeta potential of PAMAM-G4 and NAC-G4 dendrimeric conjugates were determined using a dynamic light scattering based particle size analyzer (Zetasizer Nano ZS, Malvern Instruments Ltd, Worchester, UK). The samples were diluted with triple-distilled water and DLS measurements were performed in triplicate at 25 °C with a scattering angle of 173°. Three independent measurements were taken for each sample to obtain the average hydrodynamic diameter and zeta potential.[26]

2.5. Morphological evaluation

The morphological evaluation of the conjugate was done using the atomic force microscopy technique with an NX 12 atomic force microscope (Park Systems, Suwon, Korea). A small amount of the NAC-G4 conjugate was placed on mica discs and dried. The dried sample was observed under the microscope at a cantilever frequency of 323 Hz and a scan rate of 0.5 Hz. Data analysis was performed using Park Systems XEI software, and various statistical parameters were obtained.

2.6. HPLC method for the determination of DPZ

The DPZ concentrations in the study samples were determined using an Agilent 1260 Infinity II HPLC system (Agilent Technologies, USA). HPLC analysis was carried out on a

SunFire® C18 column (4.6 × 250 mm, 5 μm) using 45 parts of ACN and 55 parts of ammonium acetate buffer (pH 6.5) as the mobile phase at a flow rate of 1 mL min^{-1} in an isocratic mode. The samples were filtered using membrane filters having a pore size of 0.22 μm and analyzed at 268 nm. The data were processed with Agilent OpenLab software.

2.7. Drug loading and entrapment efficiency

DPZ was loaded onto PAMAM-G4 and NAC-G4 conjugates using the equilibrium solubility method. Briefly, the dendrimeric conjugate and DPZ (1 : 2) were dissolved in water and stirred for 72 h. The free drug was removed by dialyzing twice against water using a 7 kDa dialysis tubing. Entrapment efficiency and drug loading were calculated using the following equations.

$$EE = \frac{\text{amount of entrapped drug}}{\text{amount of added drug}} \times 100$$

$$DL = \frac{\text{amount of entrapped drug}}{\text{total weight of drug loaded conjugate}} \times 100$$

2.8. Drug release studies

The release of DPZ from DPZ-G4 and DPZ-NAC-G4 was determined in phosphate-buffered saline (PBS) of pH 7.4 using the dialysis bag method. Briefly, DPZ-G4 and DPZ-NAC-G4 (equi-

valent to 5 mg of DPZ) were filled into a 7 kDa dialysis tube, and both ends were sealed. The tubing was then placed in 100 mL of media and stirred using a temperature-controlled magnetic stirrer maintained at 37 ± 0.5 °C. A 1 mL aliquot was collected at 0, 0.25, 0.5, 0.75, 1, 1.5, 2, 3, 4, 6, 8, 10, 24, and 48 h and replenished with fresh media. The released drug content was determined using a validated HPLC method, and the release data were fitted into various kinetic models to determine the best-fitted release kinetics for DPZ.

2.9. Haemolytic toxicity studies

Blood was collected in a microcentrifuge tube containing the anticoagulant and subjected to centrifugation ($500g$ for 5 min at 4 °C) to separate the RBCs from the plasma. The RBCs were dispersed in PBS of pH 7.4 and washed 2–3 times by centrifugation ($500g$ for 5 min at 4 °C). The blood cells were diluted 50 times, and stock solutions were prepared at 20 times the desired concentration. Triton X-100 (1%) and PBS pH 7.4 served as positive and negative controls, respectively. 50 μL of the samples were treated with 950 μL of the RBC suspension and incubated at 37 °C for 30 minutes. The treated samples were centrifuged ($500g$ for 5 min at 4 °C), and 200 μL of the supernatant was plated in a 96-well plate, and absorbance was recorded at 540 nm using a multimode plate reader.[27]

$$\% \, \text{Haemolysis} = \frac{\text{abs}_{\text{sample}} - \text{abs}_{\text{negetive control}}}{\text{abs}_{\text{positive control}} - \text{abs}_{\text{negative control}}} \times 100$$

2.10. Cytotoxicity studies

Cytotoxicity studies were conducted on SH-SY5Y cells. Briefly, the cells were seeded in a 96-well plate (1×10^4 cells per well) in a 1 : 1 mixture of DMEM and Ham's F12k at 37 °C in a 5% CO_2 atmosphere. After incubation for 24 h, the cells were treated with DPZ, DPZ-G4 and DPZ-NAC-G4 at a DPZ concentration of 3.125, 6.25, 12.5, 25, and 50 μg mL^{-1} and incubated for another 24 h. After treatment, 10 μL of 3-[4,5-dimethyl-thialzol-2-yl]-2,5-diphenyltetrazolium bromide (MTT) solution (5 mg mL^{-1} in PBS) was added to each well, and the plates were incubated for another 4 h. Then, the MTT-containing medium was replaced with 100 μL of dimethyl sulfoxide per well. The absorbance of each well was measured using a Synergy™ multimode microplate reader (BioTek Instruments, USA) at a wavelength of 570 nm. The percent viability was used to measure the relative viability of the cells and was calculated using the following equation.[28]

$$\text{Percent viability} = \frac{\text{absorbance of test}}{\text{absorbance of control}} \times 100$$

2.11. Pharmacokinetic studies

Pharmacokinetic studies were conducted on healthy male SD rats, and the rats were fasted overnight and allowed free access to diet after 4 h of dosing. The schematic representation of pharmacokinetic studies is given in Fig. 2. The animals were divided into two groups ($n = 6$); group I received DPZ-NAC-G4, and group II received DPZ (10 mg per kg body weight), orally using gastric gavage. The rats were anesthetized using isoflurane, and blood samples were withdrawn from the retro-orbital
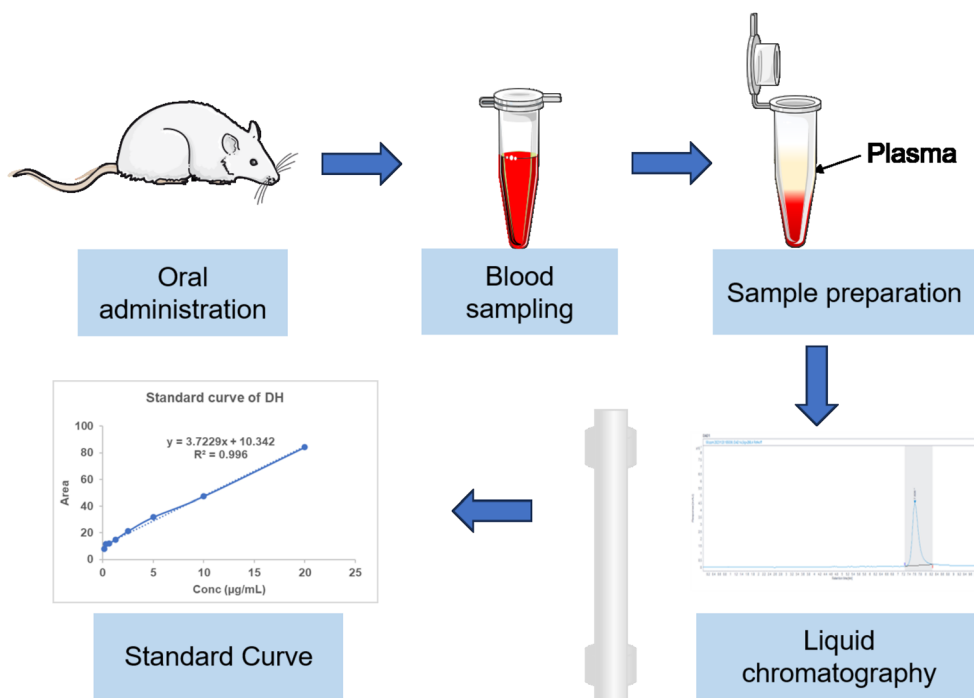

Fig. 2 Schematic representation of the pharmacokinetic studies.

plexus at 0, 1, 2, 4, 8, 12, 24, 48, 72, and 96 h in EDTA-coated microcentrifuge tubes. The blood samples were centrifuged at 1500 rpm for 10 minutes at 4 °C, and the plasma was stored at −40 °C until further analysis. DPZ was extracted from the plasma samples by the protein precipitation method using 200 μL of methanol as the precipitating solvent, and the samples were analyzed using the validated bioanalytical method. The maximum plasma concentration (C_{max}) and time to reach the maximum concentration (T_{max}) were read directly from the plot of time *vs.* plasma concentration. Area under the plasma concentration–time curve ($AUC_{0 \to t}$) was calculated using the trapezoidal method. Data were expressed as mean ± SD. The relative bioavailability (F) of DPZ from DPZ-NAC-G4 *vs.* naïve DPZ was calculated by using the given formula.[29]

$$\%F = \frac{AUC_{sample}}{dose_{sample}} \times \frac{dose_{oral}}{AUC_{oral}} \times 100$$

2.12. Estimation of DPZ in plasma

Estimation of DPZ in plasma was done by HPLC using the mobile phase consisting of phosphate buffer, methanol, and acetonitrile (50:40:10 by volume) in the isocratic mode at a flow rate of 1 mL min⁻¹. The elution was performed using a SunFire® C18 column (4.6 mm × 250 mm, 5 μm) as the stationary phase with a column oven temperature of 40 °C. All the samples were filtered through a 0.45 μm membrane prior to injection. The samples were analyzed at 268 nm using Agilent OpenLab software.

2.13. Statistical analysis

Data analysis was performed using GraphPad Prism software. The data of haemolytic toxicity, cell viability and pharmacokinetic studies are presented as mean ± SEM. One-way analysis of variance was used for statistical data analysis, where $p < 0.05$ was considered significant.

3. Results and discussion

3.1. FTIR spectra

The conjugate was characterized by FTIR spectroscopy and the FTIR spectra of PAMAM G4, NAC and NAC-G4 are shown in Fig. 3. The FTIR spectrum of PAMAM G4 showed characteristic bands at 3320 cm⁻¹ (N–H stretching), 2943 and 2835 cm⁻¹ (C–H stretching), 1637 cm⁻¹ (C=O stretching of amides), 1560 cm⁻¹ (N–H bending), 1450 cm⁻¹ (C–H bending), and 1126 cm⁻¹ and 1020 cm⁻¹ (C–N). On the other hand, the FTIR spectrum of NAC showed bands at 3430 cm⁻¹ (O–H stretching), 3375 cm⁻¹ and 3113 cm⁻¹ (N–H stretching), 3015 cm⁻¹ (C–H stretching), 2537 cm⁻¹ (S–H stretching), 1711 cm⁻¹ (C=O stretching of carboxylic acids), 1580 cm⁻¹ and 1500 cm⁻¹ (N–H bending), and 1400 cm⁻¹ (–COO symmetric vibration). The characteristic peaks in the FTIR spectrum of the NAC-G4 conjugate were observed at 3445 cm⁻¹ and 3364 cm⁻¹ (N–H stretching of primary amines), 3295 cm⁻¹ (N–H stretching of
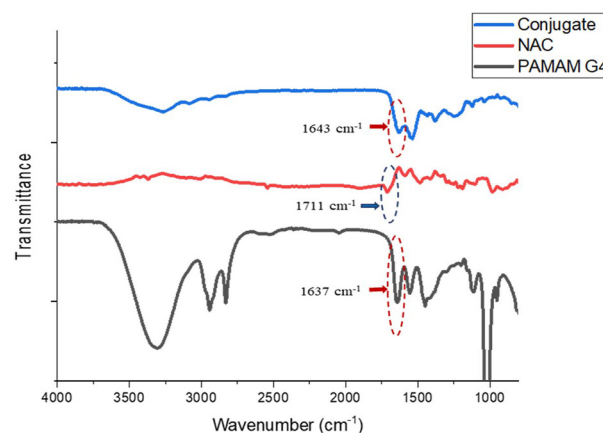

Fig. 3 FTIR spectra of PAMAM G4, NAC and the NAC-G4 conjugate.

secondary amines), 2982 cm⁻¹ (aliphatic C–H stretching), 1643 cm⁻¹ (C=O stretching of amides), 1602 and 1522 cm⁻¹ (N–H bending), 1396 cm⁻¹ (C–H bending) and 1234 cm⁻¹ (C–O). The transmittance of the N–H stretching peaks of PAMAM G4 was relatively decreased, which may be caused by the NAC modification on the terminal amine groups of PAMAM G4 dendrimers. Furthermore, the disappearance of the band at 3430 cm⁻¹ (O–H stretch) in NAC and the displacement of the band from 1711 cm⁻¹ to 1643 cm⁻¹ in NAC established the formation of the NAC-G4 conjugate *via* an amide bond.

3.2. NMR spectra

The resultant product was further characterized for the formation of the conjugate by ¹H NMR spectroscopy (JEOL RESONANCE ECZ500R, JEOL Ltd, Tokyo, Japan). The major chemical shift values in the ¹H NMR spectra of PAMAM G4, NAC and the NAC-G4 conjugate were as follows. PAMAM G4: δH-3.974 (–NH₂) and δH-7.969 (–CONH) (Fig. 4A); NAC: δH-1.84 (–CH₃), δH-4.33 (–CH, methine), δH-8.36 (–CONH, secondary amide), and δH-12.82 (–COOH) (Fig. 4B); and the NAC-G4 conjugate: δH-1.81 (–CH₃), δH-4.25 (–CH, methine), δH-7.79 (–CONH, primary), and δH-8.56 (–CONH, secondary) (Fig. 4C). The conjugate displayed a characteristic shift at 8.56 ppm (–CONH, secondary), indicating the formation of an amide linkage between the carboxylic acid group of NAC and the primary amine group of the dendrimer. The presence of NMR shifts at 1.81 ppm (–CH₃) and 4.25 ppm (–CH) and the absence of a carboxylic proton at 12.82 ppm confirm the conjugation of NAC to PAMAM G4.

3.3. Dynamic light scattering studies

The size of the dendrimeric conjugates was measured using DLS and the observed hydrodynamic diameters of PAMAM G4 and the NAC-G4 conjugate were 4.57 ± 0.11 and 260.90 ± 4.31 nm, respectively (Fig. 5). The size of the synthesized NAC-G4 was increased several fold in comparison with PAMAM G4, and this increase could be due to the formation of
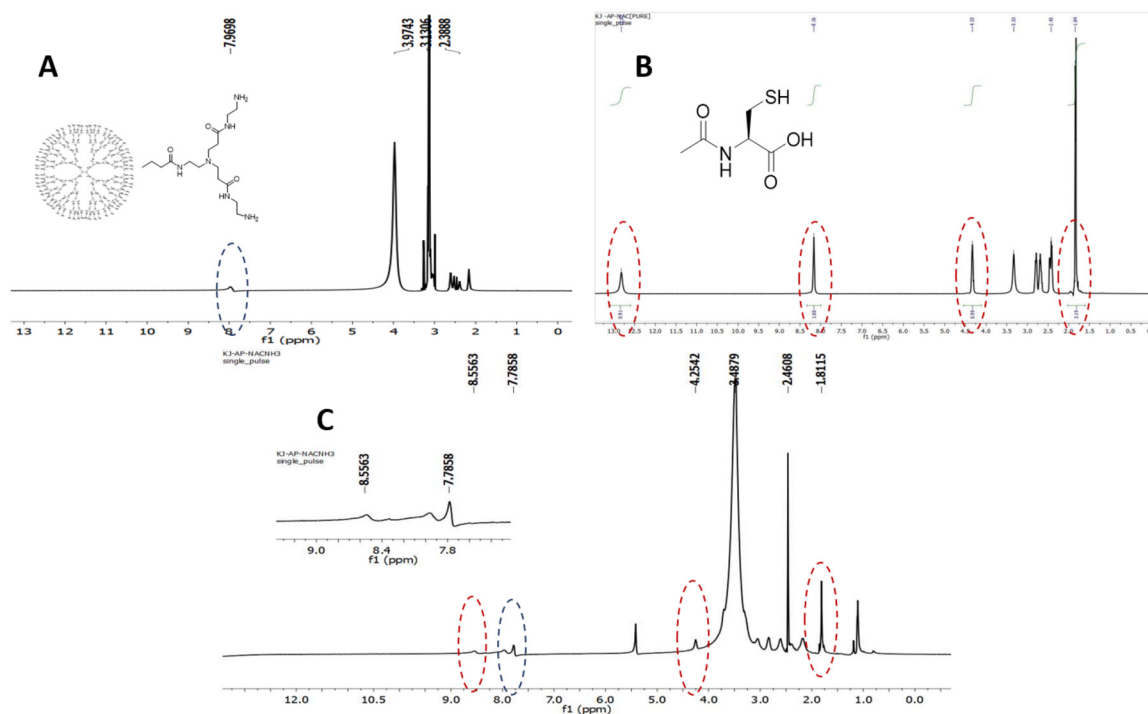
Fig. 4 NMR spectra of PAMAM G4 (A), NAC (B) and the NAC-G4 conjugate (C) in deuterated dimethyl sulfoxide.
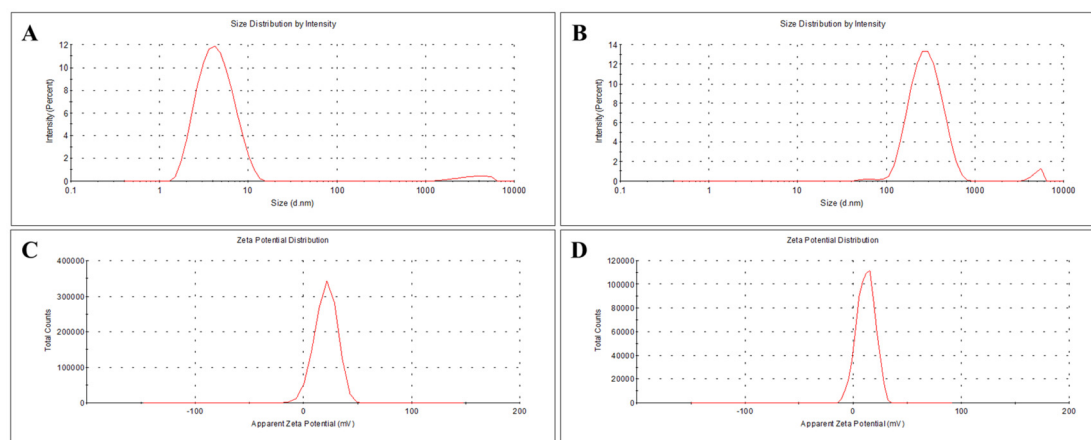

Fig. 5 DLS data representing the particle size analysis of PAMAM G4 and the NAC-G4 conjugate (A and B), zeta potential of PAMAM G4 and the NAC-G4 conjugate (C and D).

the conjugate and possible aggregation. The observed increase in size upon conjugation is consistent with previous studies on dendrimeric conjugates, where surface functionalization led to an increase in hydrodynamic diameter due to steric hindrance and partial aggregation.[30–32] The apparent zeta potential of PAMAM G4 and the NAC-G4 conjugate were 19.50 ± 3.59 and 12.33 ± 1.38 mV. The zeta potential was significantly decreased after conjugation with NAC, which is in accordance with the previous report.[33] Furthermore, the reduction in the zeta potential indicates that surface conjugation with NAC

could decrease the cationic charge over PAMAM G4 and reduce the associated toxicities.

3.4. Morphological evaluation

AFM micrographs were acquired to obtain topological information about the NAC-G4 conjugate using non-contact AFM. Fig. 6 shows typical AFM micrographs captured on exposing the mica surfaces to the synthesized NAC-G4 conjugate. The mica surfaces are essentially smooth and featureless, whereas the AFM images showed a set of isolated features, indicating
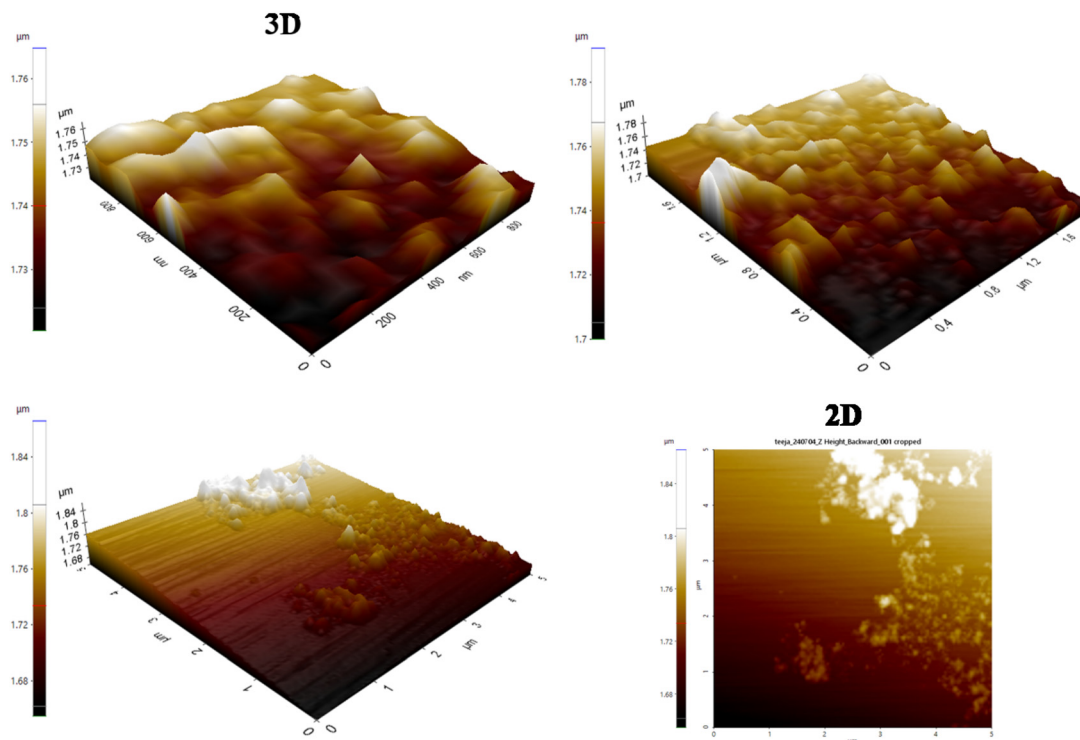
Fig. 6 Atomic force microscopy 2D and 3D images of the NAC–G4 conjugate adsorbed on mica surfaces.
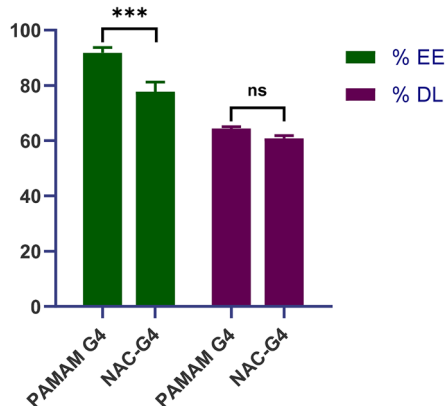

Fig. 7 Entrapment efficiency and drug loading in PAMAM G4 and the NAC–G4 conjugate (data presented as mean $\pm$ SD, n = 3). Data were analyzed using two-way ANOVA followed by Tukey's multiple comparisons test (ns: statistical insignificance; ***: $p < 0.001$).

3.5. Drug loading and entrapment efficiency

The entrapment efficiency and loading of DPZ in PAMAM G4 and the NAC-G4 dendrimeric conjugate were determined using the indirect method, and the results are presented in Fig. 7. The entrapment of DPZ was significantly higher in unmodified PAMAM G4 dendrimers in comparison with the NAC-G4 conjugate ($p < 0.001$). A similar trend was observed for drug loading, where the difference was apparent but not significant. We predict that the lower entrapment and loading could be due to the addition of ligand NAC onto the surface of PAMAM dendrimers and the steric hindrance, which potentially reduced the availability of internal cavities and surface amines for DPZ loading.

3.6. Drug release studies

The release of DPZ from the dendrimeric conjugate was determined at physiological pH, and the results are shown in Fig. 8. The release of DPZ from the dendrimeric conjugate occurred in a biphasic pattern *i.e.*, burst release in the initial 4 h followed by slow and sustained release, whereas the release was faster in case of the pure drug. The initial burst release could be attributed to the adsorbed/adhered drug on the dendrimeric surfaces. It was observed that 85.17 $\pm$ 7.47% DPZ was released from DPZ-NAC-G4 in PBS of pH 7.4 in 72 h, whereas more than 85% DPZ was released from pure drug solution within 4 h. The drug release from DPZ-G4 was slowest among all, with only 56.15 $\pm$ 7.99% release in 72 h. The conjugation of NAC over the surface of PAMAM dendrimers introduces thiol
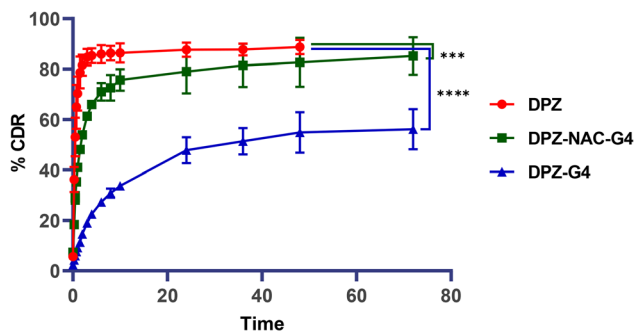
the successful adsorption of NAC-G4 over mica sheets. The root-mean-square roughness (R_{q}) and surface roughness (R_{a}) of the NAC-G4 conjugate were found to be 37 nm and 30 nm, respectively, and the Skewness and Kurtosis values were 0.191 and 2.61, respectively. The R_{q} and R_{a} values indicated very rough and highly irregular surfaces, which could be attributed to the conjugation of NAC over the surfaces of PAMAM dendrimers. High Skewness and Kurtosis values also indicated a height larger than average and a greater-pitched peak surface, respectively.[30,34]

Fig. 8 *In vitro* release profiles of DPZ from DPZ-NAC-G4, DPZ-G4 and pure drug samples in PBS (pH 7.4) at 37 °C (data presented as mean ± SD, *n* = 3). Data were analyzed using one-way ANOVA followed by Dunnett's multiple comparisons test (***: *p* < 0.001; ****: *p* < 0.0001).

Fig. 9 Haemolytic toxicity studies of DPZ, the dendrimeric conjugate and DPZ loaded conjugates (data presented as mean ± SEM, *n* = 3).

and carboxyl functional groups that alter the surface charge, hydrophilicity, and steric hindrance. This conjugation weakens the interaction between PAMAM and DPZ, leading to faster drug dissociation.

The release data from the first phase of drug release were fitted into various kinetic models and the correlation coefficient values are presented in Table S1. The *in vitro* release of DPZ from the DPZ-NAC-G4 dendrimeric conjugate was best explained by Higuchi (R^2 = 0.9822) followed by the Korsmeyer–Peppas (R^2 = 0.9761) kinetic model. The release of DPZ from DPZ-NAC-G4 was governed by Fickian diffusion.[31]

The conjugation of NAC to PAMAM dendrimers enhances the oral bioavailability and BBB penetration of DPZ by improving drug solubility, absorption, and stability. The faster release following the Higuchi kinetic model ensures controlled, sustained drug release, leading to higher brain uptake and reduced peripheral side effects, thereby enhancing the brain targeting efficiency of DPZ.

3.7. Haemolytic toxicity studies

Haemolytic toxicity associated with PAMAM dendrimers poses an obstacle in their use as drug delivery nanocarriers. Polycationic charges over the dendrimeric surfaces due to the terminal amine groups restrict their applications *in vivo*. Therefore, haemolytic toxicity studies were carried out to determine the effect of DPZ, PAMAM G4, NAC-G4, DPZ-G4 and DPZ-NAC-G4 on RBCs. The haemolytic toxicity in the current study was measured in terms of % RBC haemolysis. The results revealed that PAMAM G4 and NAC-G4 showed 5.89 ± 1.57 and 3.61 ± 0.66% RBC haemolysis, respectively, at the maximum selected concentration (100 μg mL^{-1}) (Fig. 9). Although no statistically significant differences were observed among the groups, an apparent trend indicating reduced haemolysis upon ligand conjugation was clearly visible. The results clearly projected that conjugation of the ligand over the dendrimeric surfaces condensed the RBC haemolysis substantially. The functionalization of PAMAM G4 with NAC effectively masked the primary amine groups present on the dendrimer periphery, thus reducing the toxicity of the conjugates in com-
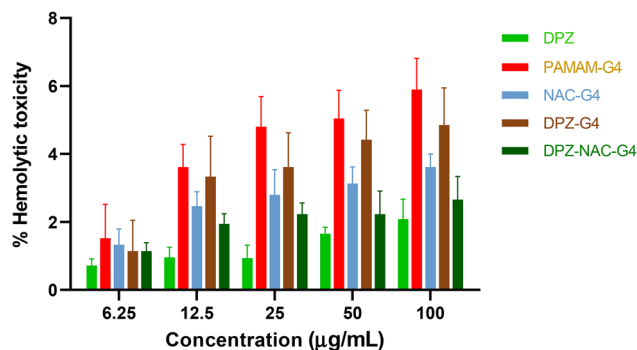
parison with PAMAM G4. The vivid reduction in the hemolytic toxicity suggests the utility of these conjugates as a convenient tool for drug delivery. Furthermore, the free drug showed 2.08 ± 1.02% haemolysis, while DPZ-G4 and DPZ-NAC-G4 showed 4.85 ± 1.89 and 2.66 ± 1.16% haemolysis, respectively (Fig. 9). While differences were not statistically significant, the trend toward decreased haemolysis with NAC functionalization supports the biocompatibility potential of the modified dendrimers. Collectively, the results indicated a substantial reduction in the haemolytic toxicity of PAMAM dendrimers on surface functionalization with NAC.[32,35]

3.8. Cytotoxicity studies

The effect of the dendrimeric conjugate and DPZ-loaded conjugate on the viability of SH-SY5Y cells was evaluated using the MTT assay. The results of the MTT assay are shown in Fig. 10, where we observed that functionalization of the dendrimers can effectively reduce the cytotoxic effects of the dendrimers. The viability of DPZ at a concentration of 50 μg mL^{-1} was 57.99 ± 1.574%, whereas upon incorporation of DPZ in dendrimeric systems, the cell viability increased to 58.75 ± 8.124% and 71.67 ± 2.608% for DPZ-G4 and DPZ-NAC-G4, respectively. Although these differences were not statistically significant, a clear trend indicating improved cell viability with NAC-functio-
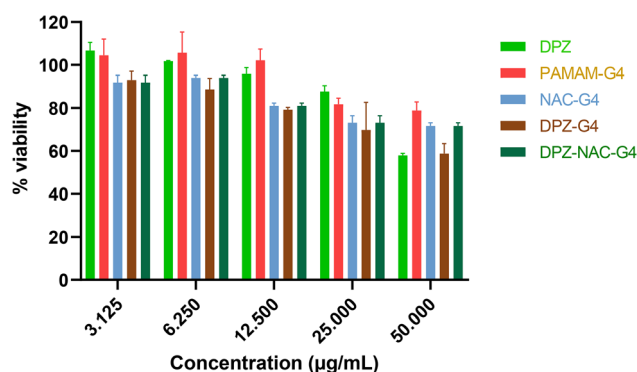

Fig. 10 *In vitro* cytotoxicity studies representing cell viability measured using the MTT assay (data presented as mean ± SEM, *n* = 3).
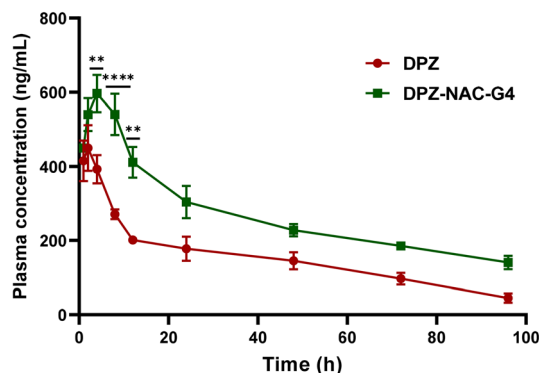
Fig. 11 Plasma concentration *vs.* time profile after oral administration (data presented as mean $\pm$ SEM, n = 5−6). Data were analyzed using two-way ANOVA followed by Sidak's multiple comparisons test (**: $p <$ 0.01; ****: $p <$ 0.0001).

nalized dendrimers was evident. The cytotoxicity values could be directly associated with the polycationic surface moieties of PAMAM G4 that causes cytotoxicity at higher concentrations of dendrimers. Surface modifications with NAC reduced these polycationic charges and thus, the cell viability increased. The results collectively indicate that incorporating DPZ in the dendrimeric conjugate could attenuate the cytotoxicity associated with DPZ.[36–38]

3.9. Pharmacokinetic studies

The pharmacokinetic studies of naïve DPZ and DPZ-NAC-G4 were performed in male SD rats and mean plasma concentration *vs.* time profile is shown in Fig. 11. After oral administration of the DPZ and DPZ loaded dendrimeric conjugate at a dose of 10 mg kg^{-1}, the drug was absorbed quickly and the pharmacokinetic profiles of DPZ and DPZ-NAC-G4 were significantly different. DPZ-NAC-G4 exhibited an ~1.4-fold and ~2.7-fold increase in peak plasma concentration (C_{max}) and time required to attain the maximum concentration (T_{max}) in comparison with DPZ solution (Table S2), indicating slow and steady absorption of the drug. Furthermore, a ~2.4-fold and ~1.8-fold increase in mean residence time (MRT) and AUC$_{0-t}$ was observed from the dendrimeric conjugate in comparison with the pure drug, which indicated the long circulating ability of the formulation in plasma. This could further aid in enhancing the brain targeting ability of the formulation and thus facilitating better therapeutic intervention in AD.

4. Conclusion

Herein, we report a systematic attempt to synthesize an NAC-G4 conjugate *via* EDC-NHS conjugation chemistry. The successful covalent linkage of NAC to PAMAM G4 dendrimers was demonstrated through FTIR and ^{1}H NMR studies. DLS studies clearly demonstrated an increase in the hydrodynamic diameter and a decrease in the apparent zeta potential of PAMAM dendrimers on conjugation with NAC. AFM analyses

revealed a rough and irregular surface of the NAC conjugated dendrimer. Release of DPZ from DPZ-G4 and DPZ-NAC-G4 occurred in a biphasic release pattern *i.e.*, burst release in the initial 4 h followed by sustained release and release was best explained by the Higuchi model. Furthermore, we observed a substantial reduction in the haemolytic toxicity and cytotoxicity of PAMAM dendrimers on surface functionalization with NAC, and the toxicities further reduced on DPZ loading. Pharmacokinetic studies showed enhanced C_{max}, T_{max}, $t_{1/2}$ and MRT values of DPZ from DPZ-NAC-G4, which could imply enhanced drug concentrations reaching the brain. In conclusion, conjugation with NAC could aid in brain targeted delivery of drugs and reduce the associated toxicities. We predict that this kind of surface-functionalized dendrimer will have exciting application prospects in various biomedical applications.

Author contributions

KJ conceptualized and supervised this research and helped in managing the required resources. TS and KJ designed the study plan; TS contributed to experimental investigation, data collection and analysis; TS wrote the manuscript; KJ contributed to the validation and review of the manuscript. All authors have read and agreed to the final version of the manuscript.

Conflicts of interest

The authors report no conflicts of interest.

Ethical statement

All animal procedures were conducted in accordance with the Guidelines for Care and Use of Laboratory Animals and were approved by the Institutional Animal Ethics Committee (IAEC) of NIPER-Raebareli (Approval no. NIPER/RBL/IAEC/159/June 2023).

Abbreviations

Aβ	Amyloid beta
ACh	Acetyl choline
AChE	Acetyl cholinesterase
AD	Alzheimer's disease
ATCI	Acetylthiocholine iodide
BBB	Blood–brain barrier
CNS	Central nervous system
DL	Drug loading
DLS	Dynamic light scattering
DPZ	Donepezil hydrochloride
DTNB	5,5′-Dithiobis(2-nitrobenzoic acid)
EDC	N-Ethyl-N′-(3-dimethylaminopropyl) carbodiimide hydrochloride

EE	Entrapment efficiency
FTIR	Fourier-transform infrared
NAC	*N*-Acetyl cysteine
NAC-G4	*N*-Acetyl cysteine-poly(amidoamine) G4 dendrimeric conjugate
NFT	Neurofibrillary tangles
NHS	*N*-Hydroxy succinimide
NMR	Nuclear magnetic resonance
PAMAM	Poly(amidoamine)

Data availability

The data supporting this article have been included as part of the SI.

Supplementary information is available. The SI file contains additional characterization data, and supporting results that complement the main manuscript. See DOI: https://doi.org/10.1039/d5pm00119f.

Acknowledgements

References

1 Dementia statistics|Alzheimer's Disease International (ADI), https://www.alzint.org/about/dementia-facts-figures/dementia-statistics.

2 T. Suthar, Navneet and K. Jain, in *Nutraceuticals for Aging and Anti-Aging: Basic Understanding and Clinical Evidence*, ed. J. N. Lokhande and Y. V. Pathak, CRC Press, 1st edn, 2021, pp. 133–168.

3 C. G. Lyketsos, M. C. Carrillo, J. M. Ryan, A. S. Khachaturian, P. Trzepacz, J. Amatniek, J. Cedarbaum, R. Brashear and D. S. Miller, *Alzheimers Dement.*, 2011, 7, 532–539.

4 S. Kumar, A. Mahajan, R. Ambatwar and G. L. Khatik, *Curr. Med. Chem.*, 2024, 31, 6032–6062.

5 T. Suthar and K. Jain, *Natural Product-based Synthetic Drug Molecules in Alzheimer's Disease*, 2023, pp. 133–153.

6 Excess Deaths Associated with COVID-19, https://www.cdc.gov/nchs/nvss/vsrr/covid19/excess_deaths.htm.

7 K. Lao, N. Ji, X. Zhang, W. Qiao, Z. Tang and X. Gou, *Drug development for Alzheimer's disease: review*, 2018, 27, pp. 164–173.

8 Z. S. Saify and N. Sultana, *Role of acetylcholinesterase inhibitors and alzheimer disease*, Elsevier, 2014, pp. 387–425.

9 P. Anand, B. Singh and N. Singh, *Bioorg. Med. Chem.*, 2012, 20, 1175–1180.

10 R. Taliyan, V. Kakoty, K. C. Sarathlal, S. S. Kharavtekar, C. R. Karennanavar, Y. K. Choudhary, G. Singhvi, Y. Riadi, S. K. Dubey and P. Kesharwani, *J. Controlled Release*, 2022, 343, 528–550.

11 B. E. Glynn-Servedio and T. S. Ranola, *Consult. Pharm.*, 2017, 32, 511–518.

12 Q. Li, S. He, Y. Chen, F. Feng, W. Qu and H. Sun, *Eur. J. Med. Chem.*, 2018, 158, 463–477.

13 R. T. Kareem, F. Abedinifar, E. A. Mahmood, A. G. Ebadi, F. Rajabi and E. Vessally, *RSC Adv.*, 2021, 11, 30781–30797.

14 I. Baysal, G. Ucar, M. Gultekinoglu, K. Ulubayram and S. Yabanoglu-Ciftci, *J. Neural Transm.*, 2017, 124, 33–45.

15 K. V. Krishna, G. Wadhwa, A. Alexander, N. Kanojia, R. N. Saha, R. Kukreti, G. Singhvi and S. K. Dubey, *ACS Chem. Neurosci.*, 2019, 10, 4124–4135.

16 R. Gauro, M. Nandave, V. K. Jain and K. Jain, *J. Nanopart. Res.*, 2021, 23, 1–20.

17 H. Kheraldine, O. Rachid, A. M. Habib, A. E. Al Moustafa, I. F. Benter and S. Akhtar, *Adv. Drug Delivery Rev.*, 2021, 178, 113908.

18 S. Sonam, P. Patel and K. Jain, *Opt. Laser Technol.*, 2024, 175, 110761.

19 A. Pathak and K. Jain, *Polymer-Drug Conjugates: Linker Chemistry, Protocols and Applications*, 2023, pp. 315–345.

20 A. K. Singh, A. Gothwal, S. Rani, M. Rana, A. K. Sharma, A. K. Yadav and U. Gupta, *ACS Omega*, 2019, 4, 4519–4528.

21 G. R. Topal, M. Mészáros, G. Porkoláb, A. Szecskó, T. F. Polgár, L. Siklós, M. A. Deli, S. Veszelka and A. Bozkir, *Pharmaceutics*, 2020, 13, 38.

22 G. İğdeli, L. Fritzen, C. U. Pietrzik and B. A. Temel, *Pharm. Dev. Technol.*, 2024, 29, 1111–1120.

23 R. B. Shahripour, M. R. Harrigan and A. V. Alexandrov, *Brain Behav.*, 2014, 4, 108.

24 M. Scalise, L. Pochini, L. Console, M. A. Losso and C. Indiveri, *Front. Cell Dev. Biol.*, 2018, 6, 96.

25 S. Asiaei, B. Smith and P. Nieva, *Biomicrofluidics*, 2015, 9, 064115.

26 V. P. Pardhi, T. Suthar, A. Sharma and K. Jain, *Nanomedicine*, 2022, 17, 1529–1546.

27 N. Singh, S. K. Sahoo and R. Kumar, *Mater. Sci. Eng., C*, 2020, 109, 110645.

28 R. C. Sahu, T. Suthar, D. Kumar, P. Singh, A. K. Datusalia and K. Jain, *J. Drug Delivery Sci. Technol.*, 2024, 92, 105336.

29 V. P. Pardhi, P. Patel, A. Vaish and K. Jain, *J. Drug Delivery Sci. Technol.*, 2024, 91, 105253.

30 A. Gothwal, K. T. Nakhate, A. Alexander, A. Ajazuddin and U. Gupta, *Mol. Pharm.*, 2018, 15, 4538–4549.

31 D. E. Igartúa, C. S. Martinez, C. F. Temprana, S. d. V. Alonso and M. J. Prieto, *Int. J. Pharm.*, 2018, 544, 191–202.

32 Y. Lu, S. Han, H. Zheng, R. Ma, Y. Ping, J. Zou, H. Tang, Y. Zhang, X. Xu and F. Li, *Int. J. Nanomed.*, 2018, 13, 5937.

33 M. Kubovcikova, R. Sobotova, V. Zavisova, I. Antal, I. Khmara, M. Lisnichuk, Z. Bednarikova, A. Jurikova, O. Strbak, J. Vojtova, P. Mikolka, J. Gombos, A. Lokajova, Z. Gazova and M. Koneracka, *Int. J. Mol. Sci.*, 2023, **24**, 11414.

34 V. Kumar, M. Rana, A. K. Sharma, S. Sinha, Ajazuddin and U. Gupta, *J. Drug Delivery Sci. Technol.*, 2023, **89**, 105058.

35 D. Bhadra, A. K. Yadav, S. Bhadra and N. K. Jain, *Int. J. Pharm.*, 2005, **295**, 221–233.

36 T. K. Rabelo, F. Zeidán-Chuliá, L. M. Vasques, J. P. A. dos Santos, R. F. da Rocha, M. A. d. B. Pasquali, J. L. Rybarczyk-Filho, A. A. S. Araújo, J. C. F. Moreira and D. P. Gelain, *Toxicol. in Vitro*, 2012, **26**, 304–314.

37 M. A. Martínez, J. L. Rodríguez, B. Lopez-Torres, M. Martínez, M. R. Martínez-Larrañaga, J. E. Maximiliano, A. Anadón and I. Ares, *Environ. Interact.*, 2020, **135**, 105414.

38 T. Suthar, P. Patel, P. Singh, A. K. Datusalia, A. K. Yadav and K. Jain, *J. Drug Delivery Sci. Technol.*, 2023, **80**, 104166.